Planetary and Space Science 58 (2010) 671–681

Contents lists available at ScienceDirect

Planetary and Space Science

journal homepage: www.elsevier.com/locate/pss

Field testing of robotic technologies to support ground ice prospecting in martian polygonal terrain

Timothy D. Barfoot [a,*], Paul T. Furgale [a], Gordon R. Osinski [b], Nadeem Ghafoor [c], Kevin K. Williams [d]

[a] University of Toronto Institute for Aerospace Studies, 4925 Dufferin Street, Toronto, Ontario, Canada M3H 5T6
[b] University of Western Ontario, Depts. of Earth Science, Physics and Astronomy Canada
[c] MDA Space Missions, Toronto Canada
[d] Buffalo State College (SUNY), Department of Earth Sciences USA

ARTICLE INFO

Article history:
Received 28 January 2009
Received in revised form
7 September 2009
Accepted 29 September 2009
Available online 6 October 2009

Keywords:
Planetary exploration
Ground-penetrating radar
Lidar
Stereo camera
Planetary rover
Analogue studies

ABSTRACT

Polygonal terrain, a landform commonly associated with the presence of ground ice, is widespread throughout the high latitudes on Mars. In this paper, we present the results of field testing a potential mission concept for the robotic prospecting of ground ice in polygonal terrain. The focus of the paper is on the key robotic technologies that could be used to implement the concept and the engineering lessons we learned (as opposed to the specific scientific findings of our field tests). In particular, we have found that a lander- or rover-mounted lidar and a rover-borne stereo camera/ground-penetrating radar suite are two important scientific tools that may be used to help pin-point ground ice prior to subsurface sampling. We field tested some aspects of this mission concept on a previously - unstudied polygonal terrain site on Devon Island in the Canadian High Arctic (a common Mars/Moon analogue site) during the summer of 2008. This unique collaboration between technological and scientific communities has led to a deeper understanding of how such a science-driven mission could actually be implemented robotically.

1. Introduction

Mars represents one of the most important targets for the international space exploration communities in the near- to mid-term (i.e., 10–30 years) and is of particular scientific importance and interest because of the widespread evidence for the presence of water in the geological past (Carr, 1996; Masson et al., 2001). Environmental conditions on Mars today are such that any water reserves will be in the form of ice, either in the polar caps or as ground ice at lower latitudes (Carr, 1996).

In addition to spectroscopic (Boynton and GRS Team, 2002) and numerically - simulated (Mellon et al., 1997) evidence for present-day ice presence, the Martian surface displays a variety of landforms similar to those indicative of ground ice in terrestrial polar regions. For example, polygonal terrain (a network of interconnected trough-like depressions in the ground) is a landform commonly found throughout the polar regions of both Earth (Lachenbruch, 1962; Mackay and Burn, 2002; Fortier and Allard, 2004a) and Mars (Mangold, 2005; Levy et al., 2009). In terrestrial environments, these features are formed by the response of an ice-bonded substrate to thermal forcing mechanisms induced by winter freezing and subsequent warming later in the season and are often indicative of subsurface ice bodies (Lachenbruch, 1962); on Mars, it is believed that such thermal forcing mechanisms may also be responsible for the observed formations (Levy et al., 2009; Mellon et al., 2008).

On Mars, the recent Phoenix mission (Smith et al., 2008) appears to have confirmed the presence of an ice-bonded substrate in polygonal terrain, but the nature of underlying massive ice bodies has not yet been determined. While earlier research has suggested that Martian polygonal terrain could potentially be representative of subsurface ice wedges (Seibert and Kargel, 2001; Mangold, 2005), more recent work has suggested that the landforms observed on the present-day Martian surface are more likely similar to 'sublimation-type' polygons (e.g., Levy et al., 2008, 2009), a type of modified sand wedge polygon reminiscent of those in the Antarctic Dry Valleys (Marchant et al., 2002; Levy et al., 2006; Marchant and Head, 2007) more so than to the ice wedge polygons typically found in the Canadian Arctic. However, until such determiniation is conclusively made it remains important to collect and interpret data indicative of the presence of all known terrestrial ground ice forms in preparation for any future robotic exploration of Mars, as deposits of ground ice may be key sites for future human exploration missions due to the possibility for in - situ resource utilization.

It is therefore very important to develop techniques for prospecting and detecting subsurface ground ice. Consequently, this paper presents a mission concept to carry out such prospecting using robotics, perhaps as a followon to the Phoenix mission.

* Corresponding author. Tel.: +1 416 667 7719.
E-mail address: tim.barfoot@utoronto.ca (T.D. Barfoot).

0032-0633/$ - see front matter © 2009 Elsevier Ltd. All rights reserved.
doi:10.1016/j.pss.2009.09.021

A sensor suite consisting of a lidar, stereo camera, and ground-penetrating radar is proposed to pinpoint ice deposits for subsequent sampling. It is important to note that our main objective in this paper is to provide a proof of concept of this mission architecture in the field, not to advance the current scientific understanding of polygonal terrain. The remainder of the paper is organized as follows. First, background and related work are provided. Next, our mission architecture is detailed, followed by experimental results. Conclusions and future work complete the paper.

2. Background and related work

One possibility for the detection of ground ice on both Mars and the Moon is ground-penetrating radar (GPR), which is widely used to determine subsurface structures and the distribution of ground ice based on differences in the dielectric properties of subsurface materials (Arcone et al., 2002). The GPR transmitter emits a high-energy electromagnetic pulse into the ground at frequencies generally in the range of 10–1000 MHz. When the signal encounters an interface between layers of differing permittivity, part of the energy is reflected back towards the surface while the remainder is refracted into the subjacent medium. The reflection/refraction process continues until the signal has attenuated completely or the user-defined time window—the amount of time that the GPR receiver is programmed to search for a return signal—has elapsed (Moorman et al., 2003). Based on the two-way travel time of each reflected pulse, a trace is produced illustrating a series of reflector intensities located beneath the unit, whereby the amplitude of the reflection is proportional to the relative difference in permittivity between adjacent materials (Arcone et al., 1995). When the GPR survey is conducted along a surface transect, individual traces can be combined to produce a radargram, a two-dimensional profile showing continuous subsurface reflective layers, which allows for enhanced stratigraphic interpretation.

The application of GPR to frozen terrain was pioneered by Annan and Davis (1976) (cf. Ross et al., 2005) and is becoming increasingly widespread. Given its established utility in some of Earth's most extreme environments such as Antarctica (Arcone et al., 2002) and the Canadian Arctic (dePascale et al., 2008), rover-based GPR has thus been proposed for development on a variety of planetary missions and will be included on ESA's upcoming ExoMars mission (Vago et al., 2006). While previous studies have focused primarily on hardware development and testing (Grant et al., 2003; Kim et al., 2006; Leuschen et al., 2002), understanding the physics of dielectric signal loss in Mars-type substrates (Pettinelli et al., 2007), and possible applications to Mars analogue environments (Arcone et al., 2002; Degenhardt and Giardino, 2003; Williams et al., 2005), relatively little effort has been directed towards the deployment of a GPR using a robotic platform (Barfoot et al., 2003). Fong et al. (2008) deployed a GPR using a rover, but did not specifically study ice prospecting. Furgale et al. (2009) detail a technique to build a coupled surface/subsurface model using a stereo camera and GPR, which was used in the current work to carry out ice prospecting.

Measuring surface properties and morphologies are also of critical importance to understanding geological processes. This information can help to predict the presence of ground ice in, for example, ice-wedge polygons. Surface properties can also help in interpreting coupled subsurface geophysical data. Properties such as elevation differences and grain size (e.g., sand versus boulders) are particularly important attributes that are always recorded and studied in detail during any field campaign on Earth, typically by a geologist taking measurements using tape measures and Global Positioning Systems (GPS). In addition to being time-consuming and relatively crude in terms of accuracy, this will not be possible on future rover missions.

One potential tool for measuring surface properties on planetary exploration missions is lidar (light detection and ranging), which offers the benefit of autonomy, mm- to cm-scale accuracy over km ranges, and the ability to generate highly precise three-dimensional (3D) topographic maps and images (Berinstain et al., 2003) from a stand-off distance. Lidar technology uses light to measure ranges to objects within its field of view, which allows 3D surface relief information about a spacecraft or rover's environment to be measured in detail. Time-of-flight lidars typically emit a short pulse of laser light and measure the time required for the pulse to reflect off the target and return to a detector in the unit. Range to the target is inferred using the speed of light and half the travel time of the pulse. Typically a mirror is used to steer the laser source in azimuth and elevation, thereby creating a raster image of ranges within a specified field of view. By transforming this range image from spherical coordinates to Euclidean coordinates, one obtains a three-dimensional model of the target as a survey 'point cloud'.

Lidar has been used extensively during the past few years for in-orbit space shuttle inspection (Gregoris et al., 2004) and, more recently, for autonomous satellite rendezvous (Allen et al., 2008). The use of lidar as a vision system for long-range rover navigation has also received considerable attention (Dupuis et al., 2008). Space-based and airborne lidar has many terrestrial applications, including mapping of geological structures, such as faults (Engelkemeir and Khan, 2008), forest canopies (Hudak et al., 2002; Andersen et al., 2006), and various geomorphological landforms, such as landslides and gullies (Jones et al., 2007; Engelkemeir and Khan, 2008). In terms of rover- and lander-based surface operations, ground-based lidar has been used extensively for atmospheric studies on Earth (Ishii et al., 1999) and, now, with the Phoenix mission, for Mars (Whiteway et al., 2008). Lidar has been previously shown to be successful for geological applications at the Haughton impact structure (Berinstain et al., 2003). Osinski et al. (2008) further showed the benefit of using lidar as a scientific tool to build detailed 3D models of various geological features including polygonal terrain, terraced crater walls, impact breccias, and gullies in the Haughton impact structure.

In addition to lidar, stereo vision has proven to be an invaluable tool for rover localization and three-dimensional modelling (Barfoot et al., 2006). A calibrated stereo camera is comprised of two monocular cameras that are a known and fixed separation apart (with aligned focal axes). By identifying common tie points on a target observed in the left and right images, one may use the known camera separation to triangulate for the range between the cameras and the target. Computer vision techniques allow this process to be automated. Stereo vision complements lidar imagery by working on a shorter scale but providing photorealistic texture, not just geometry. Moreover, stereo vision enables visual odometry, a key localization tool to help estimate rover motion in the presence of loose terrain (Furgale et al., 2009). Further discussion of the relative strengths of lidar and stereo vision to our mission concept are provided below.

The current work brings together the individual strengths of GPR, lidar, and stereo vision in a single mission architecture to prospect for ground ice.

3. Mission architecture

Fig. 1 depicts the top-level steps in our concept. The processes below the dashed line would take place on Earth, while those above would take place on Mars (in the case of prospecting for ice in polygonal terrain). The labels on the arrows indicate the data products that would be sent back and forth via Earth- Mars

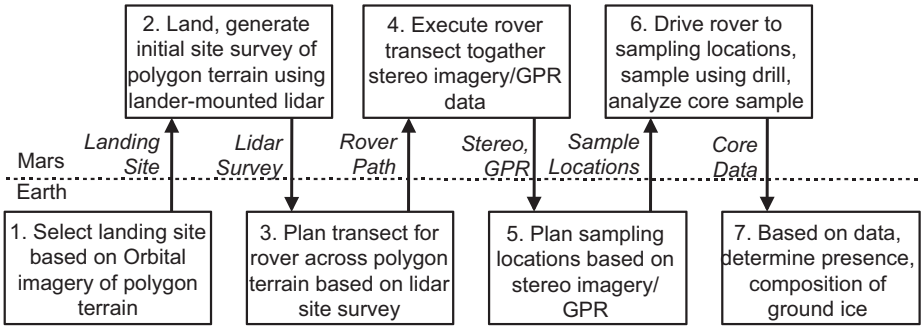

Fig. 1. Operational steps and data products transferred to/from Earth.

communications. According to this mission architecture, we first select a landing site based on orbital imagery (which can reveal the presence of polygonal terrain). We then land and build a large-scale 3D model of the surrounding terrain using a lidar on the lander.[1] We use this lidar scan to (i) select candidate polygon troughs for closer examination using stereo cameras and GPR and (ii) plan a rover path to deliver these instruments to these troughs. The rover then drives this planned path and (using a forward-looking stereo camera and GPR) builds a coupled surface/subsurface model (Furgale et al., 2009). This is enabled by a robotics technique called *visual odometry*. At select trough crossings, a second stereo camera is used to build a 360° local 3D photorealistic model, exploiting the flexibility of a mast- or robotic-arm-mounted stereo camera. The surface/subsurface model, as well as the 360° local 3D models at each trough, are used by the science team to select troughs for subsurface sampling. The rover returns to these sites (as part of the same mission), samples ground ice, analyzes the samples' composition (e.g., crystallography, isotope ratios, ice content, etc.), and returns the data to Earth.

4. Experimental setup

4.1. Field test site

The experiments described in this paper were conducted on a previously - unstudied region of polygonal terrain on Devon Island in the Canadian High Arctic, as part of Canadian Space Agency's Canadian Arctic Research Network (CARN) program (Osinski et al., 2007), and in conjunction with the Haughton-Mars Project (HMP) (Lee et al., 2007). The HMP Research Station is positioned near the northwest rim of the Haughton impact crater. Devon Island presents unique qualities for planetary analogue studies because it offers an unusually wide variety of geological features and microbiological attributes of strong planetary analogue value or potential. Devon Island is also in a polar desert environment, which presents real challenges to field exploration that are analogous in fundamental ways to those expected in planetary exploration. Devon Island has been used for rover testing in the past (Wettergreen et al., 2002; Fong et al., 2007, 2008). Our experiments were conducted approximately 10 km northeast of HMPRS near Lake Orbiter, at 75°28.937′N latitude and 89°52.138′W longitude. This site was selected based on ongoing research into the polygonal terrain it hosts. Generally, this area is comprised primarily of poorly sorted angular clasts ranging from centimeters to tens of centimeters in size. The polygonal shapes measure a few meters to tens of meters between subsequent troughs, with individual troughs averaging approximately 1–2 m in and tens of centimeters in depth.

4.2. Lander mockup

We did not simulate the actual landing/deployment portion of the mission concept, choosing instead to focus on the post-deployment operations. The lander-mounted lidar was an Optech ILRIS3D-ER with an integrated pan-tilt unit, mounted on a 3-m-high tripod (see Fig. 2(a)). We found that mounting the lidar at this height was particularly effective for capturing this scale of polygonal terrain. However, earlier experiments with a 2-m-high tripod were also successful, but to a shorter range. Hence, it is conceivable that the lidar could be mounted on a large rover rather than a lander, with little effect on our mission architecture.

4.3. Rover mockup

The rover was simulated using a push cart equipped with rover engineering sensors (i.e., stereo camera, inclinometers, sun sensor, wheel odometers), a ground-penetrating radar, an on-board computer, and two independent GPS systems (one Real-Time Kinematic) used for ground-truth positioning (see Fig. 2(b)). Although this was not a self-propelled rover, the emphasis in this work was placed on gathering the necessary scientific data products, and thus it was entirely sufficient as a means to gather data. The GPR (and cart) used was a Sensors & Software Noggin 250 MHz system (Barfoot et al., 2003). Efforts were made to minimize the effect of the rover body on the GPR data quality (e.g., using plastic parts where possible). The stereo camera used to carry out visual odometry and to help build an integrated surface/subsurface model was a Point Gray Research Bumblebee XB3 with a 24 cm baseline and 70° field of view, mounted approximately 1 m above the surface pointing downward by approximately 20°. The maximum resolution was 1280 × 960 pixels. The secondary stereo camera, used to generate 360° local 3D models, was an MDA mSM handheld system (see Fig. 2(c)).

5. Experimental results

In carrying out our experiments, we divided our personnel into an experiment team (that carried out the experiments) and a science team (that made the key mission decisions). The science team consisted of two geologists and a permafrost geomorphologist, amongst whom a total of 14 field excursions to Devon Island have been conducted. We were careful to only allow the science team access to the scientific data products that would be available on Earth during a real mission (i.e., they were not allowed to view

[1] Note that the lidar could also be mounted on a sufficiently large rover.

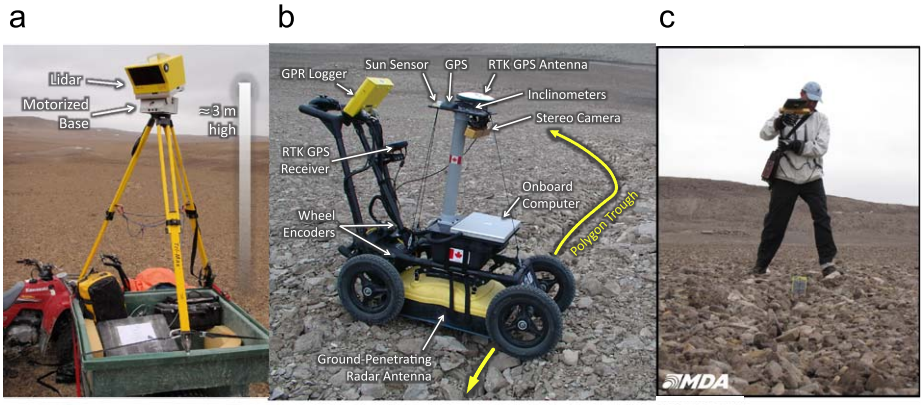

Fig. 2. Apparatus used in experiments. (a) Lander mockup. (b) Rover mockup. (c) Rover secondary stereo camera mockup.

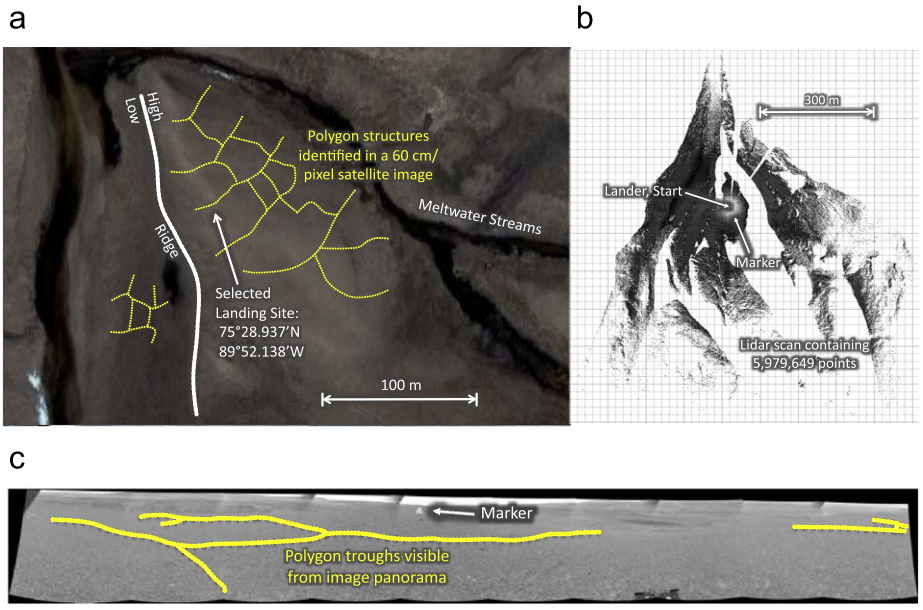

Fig. 3. Orbital image of selected landing site selection, lidar survey from lander, and image panorama from lander. (a) Orbital image. (b) Lander lidar survey. (c) Lander 360° image panorama (stitched from 10 images).

the test site in person). The remainder of this section is broken down according to the operational steps in Fig. 1.

5.1. Step 1: Select landing site

The landing site was selected in advance with the aid of a 60 cm/pixel satellite image of (a portion of) Devon Island. The image was acquired by the QuickBird Satellite and is publicly available through Google Earth. The search was narrowed to the Lake Orbiter region of Devon Island based on existing polygonal terrain studies underway in this area. However, the specific site at 75°28.937′N latitude and 89°52.138′W longitude was chosen based on our ability to discern large-scale polygonal structures in the satellite image. Note, that this specific site has not been part of any previous study. Fig. 3(a) shows the orbital image used in the landing site selection process. In the interest of clarity, the polygonal structures that can be identified (when zoomed into the image) have been marked with dotted lines.

We made no attempt to simulate the landing accuracy of an airbag or pinpoint-lidar landing system, but rather assumed the lander arrived at the desired location perfectly. In the real situation, knowledge of the landing's system accuracy would have to be acknowledged when selecting the landing site.

5.2. Step 2: Land, generate initial site survey using lidar

As mentioned above, we did not attempt to simulate the landing nor the deployment of the lander and rover, but rather chose to focus on post-deployment operations. Fig. 3(b) shows the initial lidar scan gathered at the landing site. Almost 6 million three-dimensional survey points were gathered in approximately 30 min over a 360° horizontal by 40° vertical (below horizontal) field of view. The angular resolution of the scan was 0.0688°/pixel horizontal and 0.0344°/pixel vertical. A denser vertical resolution was used due to the oblique nature of the scan above the terrain. At 3 m above the surface of the ground, the lidar was able to gather data for several hundred meters in all directions. Range was ultimately limited by the shape of the terrain rather than the sensor's capability. Note, that the lidar is able to scan at a much denser angular resolution than we used, but we found that this was not necessary to capture the essence of the polygonal terrain. Both primary and secondary polygon troughs were easily detected

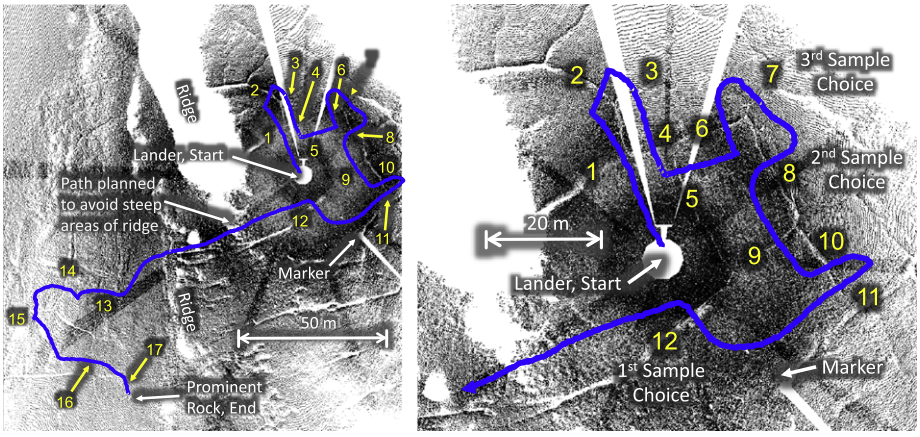

Fig. 4. Rover transect plan with 17 polygon trough crossings (based on lidar scan). (a) Full plan. (b) Closeup of start.

out to a range of over 100 m using the chosen settings. This can be better seen in Fig. 4, which zooms into the region near the lander. This fine level of detail was not available in the 60 cm/pixel orbital photograph used to select the landing site.

There are a few additional issues worth mentioning. First, a reference 'marker' was placed approximately 50 m away from the lander location. This marker was used to help determine absolute orientation of the lander (for groundtruth geo-referencing), but was not used to help acquire the science data in any way. Second, it was raining during this experiment and hence necessary to place a plastic tarp over the top of the lidar while it was scanning. Due to heavy winds, this tarp had occasion to block the lidar's scanning window twice, resulting in two small dropouts in the data, which can be seen in Fig. 3(b). Third, Fig. 3(c) shows a 360° image panorama, taken by a conventional camera included in the lidar's enclosure. Only a few primary polygon troughs could be identified clearly using this conventional image, although the resolution was fairly low ($\approx 0.1^{\circ}$/pixel). The lidar data was far superior for viewing polygonal terrain due to its three-dimensional character.

5.3. Step 3: Plan rover transect

The initial lidar site survey has both scientific and engineering merit in this mission concept. From this single data product, it is possible to identify the polygon troughs worth investigating further (using the stereo/GPR suite), but it is also possible to assess the terrain for traversability by the rover. A good example of this dual nature of the lidar data is that the science team was interested in profiling two separate polygon regions separated by a ridge. From the lidar scan, it was possible to identify a safe path for the rover to descend the ridge to the lower region (i.e., the path from trough 12 to 13). The science team planned a 350 m rover path to cross 17 polygon troughs. Figs. 4(a) and (b) show the intended rover path superimposed on the lidar scan, with the polygon troughs labelled. The traverse was planned to end at a prominent rock that could be identified in the lidar scan (see Fig. 4(a)).

5.4. Step 4: Execute transect to gather stereo/GPR

Due to logistical constraints, we did not have a self-propelled rover available for these experiments. Therefore, we were not able to test any autonomous capabilities to drive along the planned rover transect. However, by manually pushing the rover mockup (described earlier) along the planned path, we were able to gather

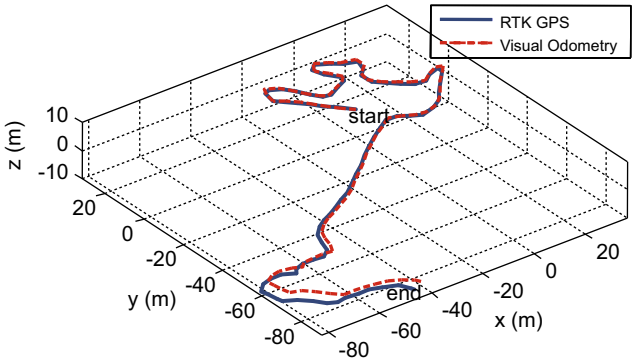

Fig. 5. Comparison of visual odometry to RTK GPS ground-truth throughout rover traverse.

both stereo imagery (every 10 cm) as well as ground-penetrating radar traces (every 5 cm). The stereo imagery was used for two purposes: (i) to carry out visual odometry (discussed briefly below) and (ii) to help build a coupled surface/subsurface model (which is described in more detail in the next section). At each trough crossing, we also gathered a more detailed three-dimensional model using the secondary stereo camera (i.e., the handheld system described earlier) that was allowed to pan/tilt in order to look sideways (i.e., down the trough) from the rover's nominal direction of travel. In the real situation, this could be accomplished using a stereo camera mounted on a robotic arm on the rover.

Visual odometry is a technique whereby the rover's relative motion is estimated primarily using images acquired from onboard (stereo) cameras. In our mission architecture, visual odometry would be used as the feedback mechanism to allow a rover to autonomous track the planned path. Although we did not close this autonomous control loop in our experiments, we did compute the visual odometry motion estimate of the manually-pushed rover cart purely from the gathered stereo images. Fig. 5 compares the computed position of the cart (using a preliminary frame-to-frame visual odometry algorithm, Furgale et al., (2009)) to our RTK GPS ground-truth measurements.

5.5. Step 5: Plan subsurface sampling locations

The output of the rover transect was a large collection of stereo imagery and GPR traces. These were processed into three

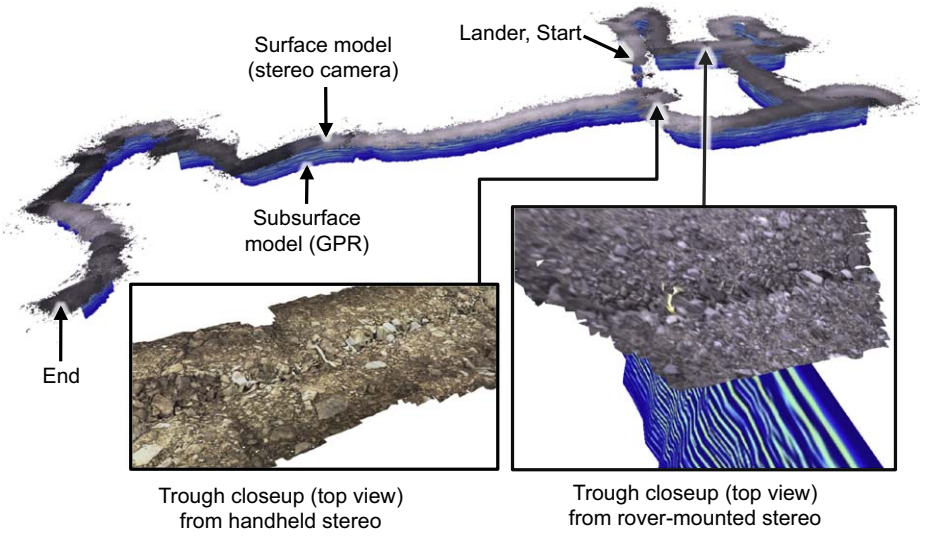

Fig. 6. Integrated surface/subsurface three-dimensional model.

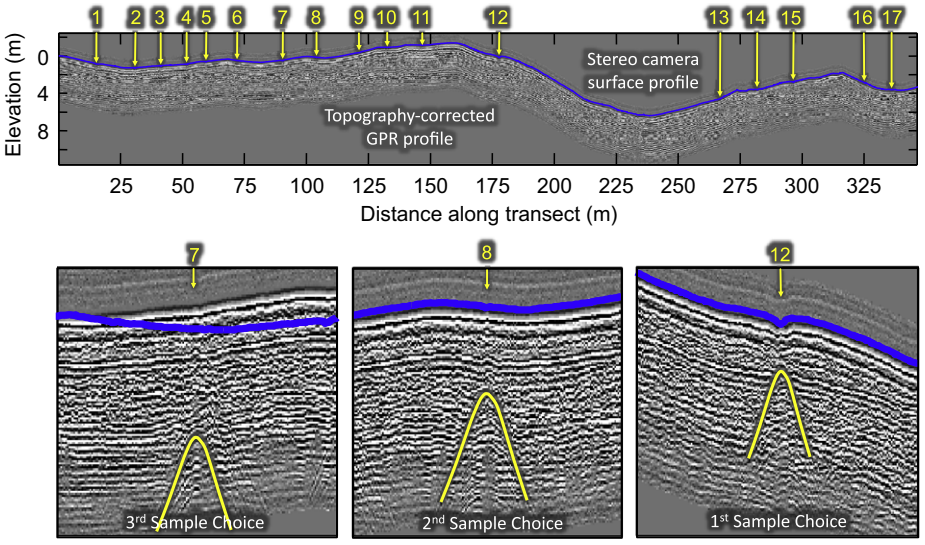

Fig. 7. Topography-corrected GPR subsurface profile with integrated surface profile from stereo camera. The clearly identiable hyperbolas have been drawn on the closeup figures for clarity. Based on this profile, troughs 12, 8, and 7 were chosen for sampling.

data products that may be used to plan subsurface sampling locations:

(1) A three-dimensional coupled surface/subsurface model of the entire transect, using the forward-looking stereo camera and GPR data (see Fig. 6).
(2) A two-dimensional coupled surface/subsurface augmented radargram of the entire transect, again using the forward-looking stereo camera and GPR data (see Fig. 7).
(3) Several local three-dimensional models of the surface of the polygon troughs crossed during the transect using the secondary stereo camera that could looks sideways down the troughs (see Fig. 6, left inset).

The three-dimensional coupled surface/subsurface model of the entire rover transect is shown in Fig. 6. The texture mapped triangle mesh of the surface (generated from stereo camera) is displayed above the ribbon of GPR data. The model may be inspected using a Virtual Reality Modeling Language viewer and rendered from any viewpoint. The technology that enables all the data to be stitched into a single model is visual odometry, which was described earlier. For further details of the surface/subsurface modeling technique, see Furgale et al. (2009).

Fig. 7 shows an augmented radargram of the entire rover transect with the 17 polygon trough crossings marked. This data product is similar to the previous one, but unfolded to be displayed in two dimensions instead of three. This radargram has been corrected for topography based on the visual odometry motion estimate described earlier (Furgale et al., 2009). As is evident, the application of topographic corrections provides a more realistic representation of subsurface stratigraphy with respect to variations in surface elevation than would an uncorrected model. Moreover, the usual GPR radargram has been augmented by adding a surface profile constructed from the stereo camera's observations of the surface. Upon zooming into this figure, it is possible to see the individual trough cross-sectional profiles (see Fig. 7).

The idea in the presented mission concept is to identify, based only on the above-mentioned data products, which polygon

troughs contain ice wedges (if any) for subsequent subsurface sampling. As noted by Hinkel et al. (2001), ice wedges "produce exceedingly complex, high amplitude hyperbolic reflections" (p. 187) due to the conical shape of the emitted GPR pulse. As a result, while ice wedges themselves are roughly triangular in shape—wider at the top and progressively narrowing with depth—their appearance on a radargram more resembles an inverted hyperbola (e.g. Hinkel et al., 2001; Fortier and Allard, 2004b). Troughs 12, 8, and 7 on Fig. 7 illustrate three such examples of hyperbolic subsurface reflections detected within the radargram.

At these and other locations along the transect, the hyperbolic reflectors are found immediately beneath the troughs as indicated by small V-shaped depressions in the stereo camera surface profile. Because polygon troughs are the most obvious surface expression of ice wedge locations (Mackay, 1999), they provide a good initial set of candidates when prospecting for ice. It should be stressed that the presence of a hyperbola does not imply a trough contains ice; hyperbolae in radargrams can also be caused by other factors such as large subsurface clasts (van Heteren et al., 1998). The only conclusion we can draw from our proof-of-concept study is that each hyperbola observed in our radar data corresponds with an overlying trough; this suggests that the complex reflections were a direct result of the wedge infill material.

The key lesson learned in this aspect of our study is that proper analysis of GPR radargrams is a difficult task at the best of times; having models of the surface to provide contextual information to aid in the interpretation of the subsurface data is critical. This topic is elaborated further in the discussion section below.

5.6. Steps 6 and 7: Extract subsurface samples, analyze

We did not have the capability to properly extract and analyze subsurface samples during our field test. Future tests should investigate the possibility of robotically deploying sampling tools and in - situ analysis instruments. Furthermore, tools such as the CRREL drill system or SIPRE permafrost corer should be used to validate the ability to pinpoint ground ice using the proposed mission concept.

6. Discussion

In this section we provide a discussion on the selection and configurations of robotic technologies we have used in our experiments to date.

6.1. Lidar vs. stereo

It is important to ask whether it is necessary to have both a lidar and a stereo camera to enable the presented ice prospecting mission scenario. In fact, we believe that the inclusion of both sensors can be justified purely on a scientific basis and that there are additional engineering reasons for having both. Lidar and stereo are fairly complementary technologies as summarized in Table 1. Under this mission scenario, we advocate for a careful survey of the site prior to any subsurface sampling. A compact version of the mission is even possible in which we forego the subsurface sampling altogether. The critical data product in both cases is the GPR transect, which gives a view of the subsurface. However, based on our experiences in the field, it is paramount to have a clear understanding of the surface to aid in the interpretation of the subsurface data produced by the GPR.

Table 1
Complementary capabilities of lidar and stereo camera sensors in our setup.

	Power	Mass	3D range	Color info?
Lidar	High	High	>1 km	No
Stereo camera	Low	Low	<10 m	Yes

We assert that to fully understand polygonal terrain, one must consider what is happening at both large (e.g., hundreds of meters) and small (e.g., tens of centimeters) scales. The large scale is important to provide the overall distribution of primary and secondary troughs and their patterns in the region around the landing site. Moreover, the surrounding terrain can provide important clues about the external influences on the terrain (e.g., topography). For example, the test site described in this paper has a fairly large variation in altitude (e.g., 10 m) that could not be accurately gleaned from the orbital imagery. The small scale is important to provide unoccluded 3D and photorealistic information about the troughs crossed by the GPR transect. This information can be used to understand the relative grain size of rocks both inside and outside the troughs, which can in turn provide key hints as to the presence of ice wedges. The question we must ask is, what is the best way to provide large and small scale contextual information in a planetary exploration setting?

At the large scale, generating useable topographic data for traverse mapping and sampling strategies using orbital data is not straightforward. The Mars Orbiter Laser Altimeter (MOLA) (Smith et al., 1999) can be used to represent landscape-scale topography, but given that individual data points are spaced at approximately 300 m, these data would be inappropriate for site-scale traverse planning. Recent advances in softcopy photogrammetric techniques using 0.25 m pixel imagery from the HiRISE camera (McEwen et al., 2007) aboard Mars Reconnaissance Orbiter (Zurek and Smrekar, 2007) represent a marked improvement, but Digital Terrain Models (DTM) generated using this methodology are limited to a resolution of approximately 1 m (Kirk et al., 2008). We therefore require a sensor on the ground to provide the large-scale contextual information.

It might be possible to use a stereo camera on a mast to build a large-scale three-dimensional model of the terrain around the landing site. From a landed platform, the Phoenix mission's (Smith et al., 2008) onboard stereo camera provides a good example of generating a detailed, localized DTM. However, while the resolution of this DTM was extremely fine—on the order of centimeters per pixel—the spatial extent was limited to approximately the first two meters from the lander. A lidar is the simplest solution to obtain large-scale information as it can build a very high-quality map from a single measurement location in a reasonably short amount of time (e.g., a few hours). As demonstrated in our experiments, a time-of-flight lidar located on the ground at the landing site is certainly capable of building a high-quality three-dimensional map of polygonal terrain that reveals both the primary and secondary troughs within a large neighbourhood of the landing site (e.g., out to 100 m).

However, the lidar scan taken from the landing location is not sufficient to provide contextual information on the small scale for three reasons: (i) there are sometimes occlusions in the polygon troughs due to the oblique nature of the lidar scan, (ii) the resolution is insufficient, particularly for far-away secondary troughs, and (iii) it does not provide colour/texture information about the terrain. It might be possible to overcome the resolution and colour/texture issues of the lidar by increasing the resolution of the scan in key regions and mapping an ultra-high-resolution colour camera image onto the lidar data. However, the occlusion issue can only be overcome by viewing the troughs from a less oblique angle (e.g., looking down from above the trough). In

contrast, a stereo camera is able to provide the required model, and has an additional engineering advantage in that it may also be used for visual odometry as discussed above. For this reason, we believe the stereo camera mounted on the rover carrying the GPR is the best option to provide small-scale information directly above the GPR transect.

In summary, we believe that both large and small scale surface information is necessary to properly interpret polygonal terrain and efficiently pinpoint ground ice. The best option to provide large-scale information is a lidar scan taken from a single location on the ground (note, that the lidar could be on a lander or the rover). The best option to provide the requisite small-scale detail above the GPR transect is a stereo camera mounted on the rover. The next sections discuss some key aspects (including ideas for metrics) of both the lidar and GPR/stereo models.

6.2. Lidar model

To build a useful topographic model of the surface using a sensor, there are typically several configuration parameters that can be varied. As described above, our lidar unit was mounted a certain distance above the ground, tilted at a particular angle, and had different vertical and horizontal angular scan resolutions. All of these settings affect the density of three-dimensional survey points on the ground. Fig. 8 shows how the density of survey points depended on the range from the lidar unit in our scan. The reason the density decreases rapidly with range is the oblique nature of the scan. Density of points on the ground (over a whole site) is probably the first metric to consider when comparing different topographic modeling options, as it is not specific to any particular type of sensor. A key question is, what is the density requirement to produce a topographic model that is good enough? This is actually difficult to answer as it depends on the type of terrain being imaged. Even for polygonal terrain, there is a good deal of variability in the width and depth of troughs. Based on the data gathered at our field site, we found that it was possible to see the primary troughs out to 100 m; the troughs were $\approx 1-2$ m wide and $\approx 0.1-0.2$ m deep, and the point density was as low as 10 points/m^2. The secondary troughs could be seen only out to about 25 m; the troughs were ≈ 0.5 m wide and ≈ 0.05 m deep, and the point density was about 100 points/m^2. A detailed study of the relationship between polygon geometry and lidar configuration parameters would allow more quantitative conclusions to be drawn.

6.3. GPR/stereo model

Our GPR traces were taken every 0.05 m along the 350 m transect, triggered by wheel odometry on the rover. This horizontal sample spacing was selected based on the frequency of the GPR, which was 250 MHz. The 250 MHz frequency was selected based on the depth of the subsurface profile we sought to construct, which was approximately 5 m. This depth was needed to see beyond the active layer, which was located at approximately 1.0 m depth at the time of sampling. In this particular polygon terrain, these parameters seemed adequate to characterize the subsurface.

Based on the stereo camera configuration used in our experiments, each stereo image pair is capable of generating approximately 72,000 points/m^2 (near the projection of the optical center on the ground). Not only is this point density higher than the lidar's at its closest range, it remains consistent throughout the rover traverse because the stereo camera's relationship to the ground remains somewhat constant. Images were captured approximately every 0.1 m along the rover traverse. Saving all of the original three-dimensional points as a surface model is possible, but not necessary as there is a good deal of redundancy in the form of overlapping imagery (this overlap is in fact what we rely on to make visual odometry work).

For the coupled three-dimensional surface/subsurface model depicted in Fig. 6, the raw survey points are fitted with a triangular mesh and overlayed with higher-resolution photorealistic textures (Furgale et al., 2009). This type of model is advantageous over simply saving all of the original three-dimensional points as the model is smoother and a fraction of the size to store. This smaller model can be transmitted much more quickly back to Earth, yet still maintains a good three-dimensional representation of the terrain as well as photorealism. Fig. 9 provides a histogram of triangle areas in the long surface model shown in Fig. 6. Many of the triangles are approximately 3–4 cm across, which is sufficient to capture the shape of the larger polygon troughs and is similar in scale to the 5 cm GPR

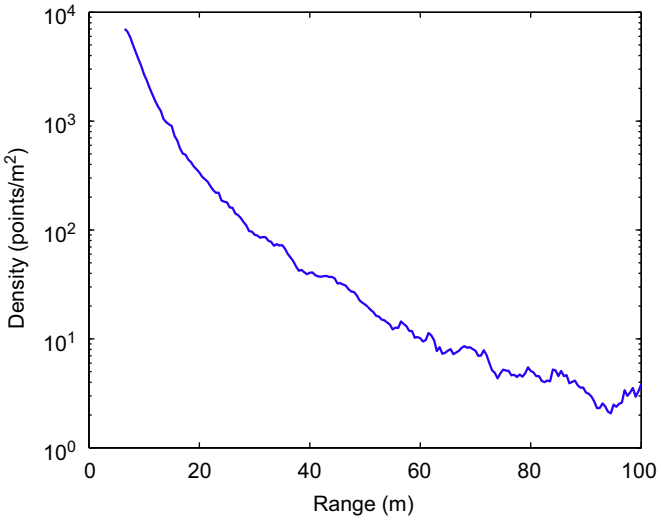

Fig. 8. Density of lidar three-dimensional survey points on the ground as a function of range from the lidar's location (for the lidar scan described in this paper).

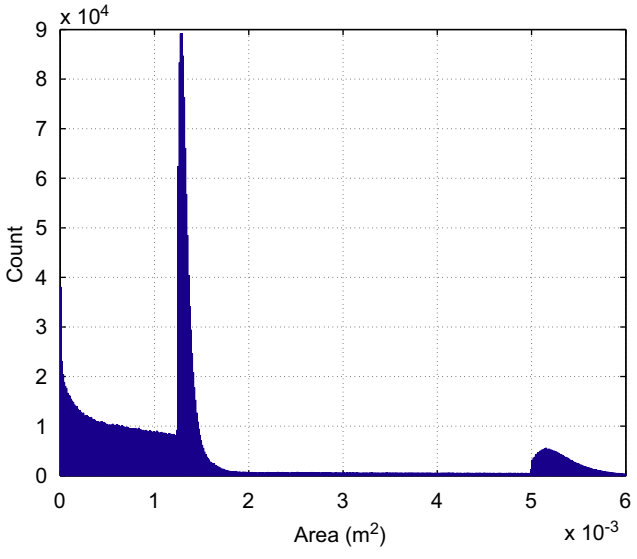

Fig. 9. Histogram of triangle areas in the stereo camera surface mesh depicted in Fig. 6. Most of the useful triangles are clustered near 0.0013 m^2 (or about 3–4 cm across).

horizontal resolution. The triangles are textured with the original high-resolution images, which means particles smaller than triangle size can still be viewed in the model.

For the two-dimensional surface profile depicted in Fig. 7, it was also advantageous to not store all the raw survey points. In this case, a spline was fit to the data, which smoothed the profile. The raw points and fitted spline may be seen for one polygon trough in Fig. 10; the trough center is located at approximately 16.5 m along the transect.

The selection of the triangle mesh and spline fitting parameters should clearly be based on the expected trough geometries in this mission concept, particularly if only the fitted models will be returned to Earth to save transmission time. A more practical approach might be to save all the raw imagery locally on the rover, send back a well-compressed model to serve as a 'thumbnail' preview, and allow requests for finer-resolution versions as needed.

6.4. Additional engineering issues

We have made a scientific case for using both a lidar and stereo camera to provide large- and small-scale information to aid in the interpretation of the subsurface data collected by the GPR in our mission concept. There are some additional engineering reasons to strengthen our position for including both sensors.

First, the map of the polygon terrain derived from the lidar can be used to plan out a GPR transect. This is critical for polygonal terrain because we want the GPR to cross the troughs as perpendicularly as possible to obtain clean returns. Without this large-scale lidar map, the rover would likely be forced to traverse in a regular grid type pattern (Fong et al., 2008), which would mean many of the troughs would not be crossed perpendicularly and thus suboptimally.

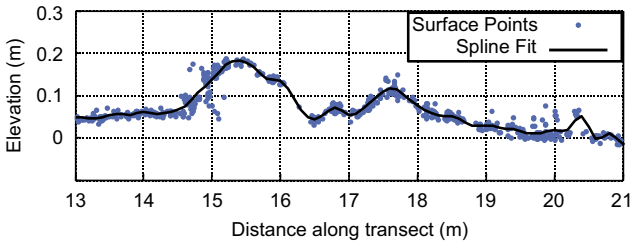

Fig. 10. Spline fit to raw survey points for two-dimensional surface profile.

Second, as discussed above in Section 5.4, in addition to enabling surface modelling, the stereo camera can be used to compute the relative motion of the rover both in position and orientation using a technique called visual odometry. This is the critical technology needed to stitch together all of the GPR traces into a single subsurface image (as well as to stitch together the three-dimensional data into a surface model). Other potential methods of localizing the rover throughout the traverse exist and should be considered. For example, placing fiducial markers on the rover and observing it from the lander is a possibility (using, for example, the lidar) (Fontaine et al., 2000). This approach would likely do a good job of coarsely estimating the rover's position over a short range. Orientation would likely need to be estimated using rate gyros in this case. However, it is unlikely that a fiducial-based system would be able to measure relative changes in position accurately enough to not introduce artifacts into the surface and subsurface models. Visual odometry is intrinsically good at measuring relative motion and thus is ideally suited to this 'stitching' localization task. Moreover, no sensing is needed in addition to the stereo camera.

One caveat to using visual odometry is that error in the motion estimate accumulates with distance travelled. Referring to Fig. 4(a), above the 'ridge', the accuracy of our visual odometry motion estimate was very good and would likely allow the rover to cross the intended polygon troughs autonomously. Below the 'ridge', the error in our motion estimate has grown to a few meters, which is similar in scale to the polygons' dimensions. It would likely be necessary to improve the accuracy of the visual odometry algorithm to allow rover transects of this length (on polygons of this size). Another possibility would be to reset the localization by matching a local three-dimenional scan (using either stereo camera or a lidar on the rover) to the initial lidar site survey. Or, the lander could observe the rover using the lidar (or vice versa) to reset the localization during the transect (i.e., using fiducial markers). We will be investigating this aspect of the mission concept in future work.

A final use for the stereo camera that is worth mentioning is as a means to backtrack along the GPR transect to sites selected for subsurface sampling. We are currently developing a visual teach-and-repeat system that requires only a stereo camera to allow a rover to be taught a route manually and then autonomously repeat (or reverse) it. This technique could be used to autonomously backtrack along the GPR transect to those troughs selected for coring. This technique will be field tested in the summer of 2009.

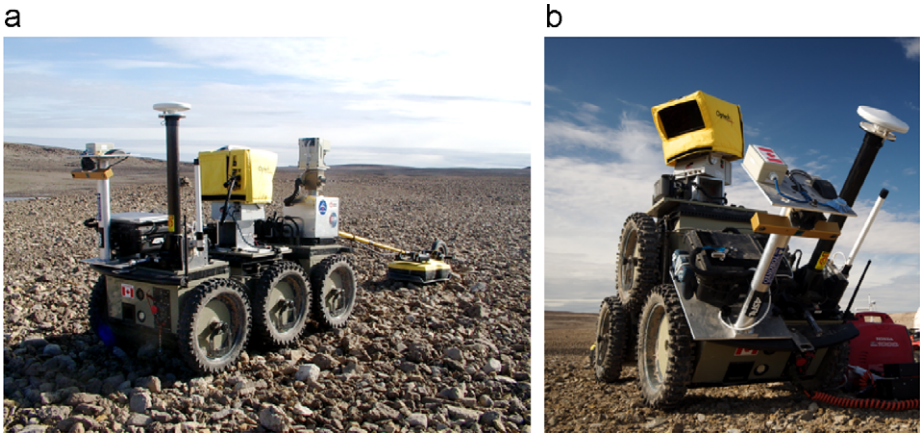

Fig. 11. Field robot used for follow-on testing on Devon Island during the summer of 2009. (a) ROC6 field robot with lidar, stereo camera, and GPR. (b) ROC6 with lidar extended vertically.

7. Conclusion and future work

We have proposed a mission concept driven by the top-level scientific objective of pinpointing and sampling ground ice in Martian polygonal terrain. This led to the initial operational concept discussed above. The main contribution of the paper is the elaboration of lessons learned regarding the robotic tools needed to implement some aspects of the proposed concept.

Based on proof-of-concept field tests conducted on Devon Island during the summer of 2008, we have shown that (i) existing lidar technology can easily map out polygon troughs to 100 m from a lander, and (ii) a subsurface model based on GPR data (as well as a coupled surface model based on stereo vision) can be automatically created from a rover platform. Future technical challenges include: GPR/rover integration, automatically driving the rover along the planned path, automatically returning the rover to the subsurface sampling sites, and automatically extracting and analyzing the subsurface samples.

We have, in fact, already conducted followon field tests on Devon Island during the summer of 2009, to address some of these additional challenges. We used the field robot depicted in Fig. 11. Notably, in this setup, the lidar is mounted on the rover rather than a lander. By mounting the lidar on the rover, the same mission concept presented here could be repeated several times, allowing the rover to traverse over the horizon away from the landing site. The results of these field tests will be presented in due course.

Acknowledgments

The authors are extremely indebted to Timothy Haltigin of McGill University, who provided invaluable advice on the incorporation of polygonal terrain processes into our mission scenario. He served on our science team and helped to select the test site, plan the rover transect based on lidar data, interpret the resulting ground-penetrating radar data, and select the subsurface sampling locations. Finally, he generously provided a critique of this manuscript, from a geomorphological perspective.

This project was made possible through the support of many organizations and individuals and the authors would like to thank each of them. Funding for our field trials on Devon Island was provided by The Canadian Space Agency's Canadian Analogue Research Network (CARN) program and the Natural Sciences and Engineering Research Council of Canada (NSERC). The Haughton-Mars Project provided infrastructure on Devon Island. Members of the communities of Resolute Bay, Grise Fjord, and Pond Inlet acted as guides. Tom Lamarche from the Canadian Space Agency helped with our field testing. Peter Annan and David Redman from Sensors & Software Inc. helped us with equipment, and offered advice on the use of GPR in the field. Patrick Carle at UTIAS developed the procedures to operate the lander lidar and Optech Inc. also provided valuable advice in this regard. Piotr Jasiobedzki and Stephen Se were instrumental in developing MDA Space Mission's Instant Scene Modeler and Ho-Kong Ng converted our motion estimates and images into surface models. Our visual odometry algorithm used the SURF library developed by Herbert Bay, Luc Van Gool and Tinne Tuytelaars and available at http://www.vision.ee.ethz.ch/~surf/. Finally, at UTIAS, Konstantine Tsotsos and Peter Miras provided logistical support, and Rehman Merali pitched in during assembly of our pushcart rover.

References

Allen, A., Langley, C., Mukherji, R., Taylor, A., Umasuthan, M., Barfoot, T., 2008. Rendezvous lidar sensor system for terminal rendezvous, capture, and berthing to the international space station. In: Proceedings of the SPIE Space Exploration Technology Conference, vol. 6958: Sensors and Systems for Space Applications II, Orlando, Florida.

Andersen, H.E., Reutebuch, S.E., McGaughey, R.J., 2006. A rigorous assessment of tree height measurements obtained using airborne lidar and conventional field methods. Canadian Journal of Remote Sensing 32, 355–366.

Annan, A., Davis, J., 1976. Impulse radar sounding in permafrost. Radio Science 11, 383–394.

Arcone, S., Lawson, D., Delaney, A., 1995. Short-pulse radar wavelet recovery and resolution of dielectric constants within englacial and basal ice of matanuska glacier, alaska, usa. Journal of Glaciology 41, 68–86.

Arcone, S., Prentice, M., Delaney, A., 2002. Stratigraphic profiling with ground-penetrating radar in permafrost: A review of possible analogs for mars. Journal of Geophysical Research 107 (E11), 5108.

Barfoot, T., D'Eleuterio, G., Annan, P., 2003. Subsurface surveying by a rover equipped with ground penetrating radar. In: Proceedings of the IEEE/RSJ International Conference on Intelligent Robots and Systems (IROS), Las Vegas, NV, pp. 2541–2546.

Barfoot, T., Se, S., Jasiobedzki, P., 2006. Visual motion estimation and terrain modelling for planetary rovers. In: Ayanna, H., Edward, T. (Eds.) (Jet Propulsion Laboratory), Intelligence for Space Robotics. TSI Press, NM, pp. 71–92 (Chapter 4).

Berinstain, A., Osinski, G.R., Spray, J.G., Lee, P., Hahn, J., Ulitsky, A., 2003. Applications of time-of-flight lidar in crater geology. In: Kamerman, G.W. (Ed.), Proceedings of the SPIE Laser Radar Technology and Applications VIII, vol. 5086, pp. 292–298.

Boynton, W.V., GRS Team, 2002. Distribution of hydrogen in the near-surface of mars: Evidence for subsurface ice deposits. Science 297, 81–85.

Carr, M.H., 1996. Water on Mars. Oxford University Press, New York.

Degenhardt, J.J., Giardino, J.R., 2003. Subsurface investigation of a rock glacier using ground-penetrating radar: Implications for locating stored water on Mars. Journal of Geophysical Research (Planets) 108, 8036.

dePascale, G., Pollard, W., Williams, K., 2008. Geophysical mapping of ground ice using a combination of capacitive coupled Resistivity and ground-penetrating radar, northwest territories, canada. Journal of Geophysical Research 113, F02S90.

Dupuis, E., Rekleitis, I., Bedwani, J.L., Lamarche, T., Allard, P., Zhu, W.H., 2008. Over-the-horizon autonomous rover navigation: Experimental results. In: Proceedings of the 9th International Symposium on Artificial Intelligence, Robotics and Automation in Space (iSAIRAS), Los Angeles, CA.

Engelkemeir, R.M., Khan, S.D., 2008. Lidar mapping of faults in houston, texas, usa. In: Geosphere 4, pp. 170–182.

Fong, T., Allan, M., Bouyssounouse, X., Bualat, M., Deans, M., Edwards, L., Fluckiger, L., Keely, L., Lee, S., Lees, D., To, V., Utz, H., 2008. Robotics site survey at haughton crater. In: Proceedings of the 9th International Symposium on Artificial Intelligence, Robotics and Automation in Space (iSAIRAS), Los Angeles, CA.

Fong, T., Deans, M., Lee, P., Bualat, M., 2007. Simulated lunar robotic survey at terrestrial analog sites. In: Proceedings of the 38th Lunar and Planetary Science Conference, League City, Texas.

Fontaine, B., Termont, D., Steinicke, L., Pollefeys, M., Vergauwen, M., Moreas, R., Xu, F., Landzettel, K., Steinmetz, M., Brunner, B., Michaelis, H., Behnke, T., Dequeker, R., Degezelle, P., Bertrand, R., Visentin, G., 2000. Autonomous operations of the micro-rover for geo-science on mars. In: Proceedings of 6th ESA Workshop on Advanced Space Technologies for Robotics and Automation (ASTRA).

Fortier, D., Allard, M., 2004a. Late holocene syngenetic ice wedge polygons development, bylot island, canadian arctic archipelago. Canadian Journal of Earth Sciences 41, 997–1012.

Fortier, D., Allard, M., 2004b. Late holocene syngentic ice-wedge polygons development, bylot island, canadian arctic archipelago. Canadian Journal of Earth Sciences 41, 997–1012.

Furgale, P.T., Barfoot, T.D., Osinski, G.R., Williams, K., Ghafoor, N., Field Testing of an Integrated Surface/Subsurface Modeling Technique for Planetary Exploration. Submitted to the International Journal of Robotics Research, invited special issue on "Field and Service Robotics" on September 29, 2009. Manuscript # IJR-09-0636.

Grant, J.A., Schutz, A.E., Campbell, B.A., 2003. Ground-penetrating radar as a tool for probing the shallow subsurface of Mars. Journal of Geophysical Research 108 (E4).

Gregoris, D.J., Ulitsky, A., Vit, D., Kerr, A., Dorcas, P., Bailak, G., Tripp, J., Gillett, R., Woodland, C., Richards, R., Sallaberger, C., 2004. Laser imaging sensor system for on-orbit space shuttle inspection. In: Spaceborne Sensors (SPIE), Orlando, FL, USA, pp. 61–68.

Hinkel, K., Doolittle, J., Bockheim, J., Nelson, F., Paetzold, R., Kimble, J., Travis, R., 2001. Detection of subsurface permafrost features with ground-penetrating radar, barrow, alaska. Permafrost and Periglacial Processes 12, 179–190.

Hudak, A.T., Lefsky, M.A., Cohen, W.B., Berterretche, M., 2002. Integration of lidar and landsat etm+ data for estimating and mapping forest canopy height. Remote Sensing of Environment 82, 397–416.

Ishii, S., Shibata, T., Nagai, T., Mizutani, K., Itabe, T., Hirota, M., Fujimoto, T., Uchino, O., 1999. Arctic haze and clouds observed by lidar during four winter seasons of 1992–1997, at eureka, canada. Atmospheric Environment 33, 2459–2470.

Jones, A.F., Brewer, P.A., Johnstone, E., Macklin, M.G., 2007. High-resolution interpretative geomorphological mapping of river valley environments using airborne lidar data. Earth Surface Processes and Landforms 32, 1574–1592.

Kim, S.S., Carnes, S., Haldemann, A., Ho Wah Ng, E., Ulmer, C., Arcone, S., 2006. Miniature ground penetrating radar, crux gpr. In: Aerospace Conference, 2006 IEEE, 7pp.

Kirk, R.L., Howington-Kraus, E., Rosiek, M.R., Anderson, J.A., Archinal, B.A., Becker, K.J., Cook, D.A., Galuszka, D.M., Geissler, P.E., Hare, T.M., Holmberg, I.M., Keszthelyi, P., Redding, B.L., Delamere, W.A., Gallagher, D., Chapel, J.D., Eliason, E.M., Kinkg, R., McEwen, A.S., 2008. Ultrahigh resolution topographic mapping of mars with mro hirise stereo images: Meter-scale slopes of candidate phoenix landing sites. Journal of Geophysical Research 113 (E00A24).

Lachenbruch, A., 1962. Mechanics of thermal contraction cracks and ice-wedge polygons in permafrost. Special paper to the Geological Society of America 70, 69.

Lee, P., Braham, S., Boucher, M., Schutt, J., Glass, B., Gross, A., Hine, B., McKay, C., Hoffman, S., Jones, J., Berinstain, A., Comptois, J.-M., Hodgson, E., Wilkinson, N., 2007. Haughton-mars project: 10 years of science operations and exploration systems development at a moon/mars analog site on devon island, high arctic. In: Proceedings of the 38th Lunar and Planetary Science Conference, League City, Texas, pp. 2426–2427.

Leuschen, C., Kanagaratnam, P., Yoshikawa, K., Arcone, S., Gogineni, P., 2002. Field experiments of a surface-penetrating radar for Mars. In: 2002 IEEE International in Geoscience and Remote Sensing Symposium, 2002. IGARSS '02, vol. 6, pp. 3579–3581.

Levy, J., Head, J., Marchant, D., 2009. Thermal contraction crack polygons on Mars: classification, distribution, and climate implications from hirise observations. Journal of Geophysical Research 114 (E01007).

Levy, J.S., Head, J.W., Marchant, D.R., Kowalewski, D.E., 2008. Identification of sublimation-type thermal contraction crack polygons at the proposed nasa phoenix landing site: implications for substrate properties and climate-driven morphological evolution. Geophysical Research Letters 25 (L04202).

Levy, J.S., Marchant, D.R., Head, J.W., 2006. Distribution and origin of patterned ground on mullins valley debris-covered glacier, antarctica: the roles of ice flow and sublimation. Antarctic Science 18 (3), 385–397.

Mackay, J., 1999. Periglacial features developed on the exposed lake bottoms of seven lakes that drained rapidly after 1950, tuktoyaktuk peninsula area, western arctic coast, canada. Permafrost and Periglacial Processes 10, 39–63.

Mackay, J.R., Burn, C.R., 2002. The first 20 years (1978–1979 to 1998–1999) of ice wedge growth at the illisarvik experimental drained lake site, western arctic coast, canada. Canadian Journal of Earth Sciences 39 (1), 95–111.

Mangold, N.A., 2005. High latitude patterned grounds on mars: Classification, distribution, and climatic control. Icarus 174, 336–359.

Marchant, D.R., Head, J.W., 2007. Antarctic dry valleys: Microclimate zonation, variable geomorphic processes, and implications for assessing climate change on mars. Icarus 192 (1), 187–222.

Marchant, D.R., Lewis, A.R., Phillips, W.M., Moore, E.J., Souchez, R.A., Denton, G.H., Sugden, D.E., Potter, N., Landis, G.P., 2002. Formation of patterned ground and sublimation till over miocene glacier ice in beacon valley, southern victoria land, antarctica. Geological Society of America Bulletin 114 (6), 718–730.

Masson, P., Carr, M.H., Costard, F., Greeley, R., Hauber, E., Jaumann, R., 2001. Geomorphologic evidence for liquid water. Space Science Reviews 96, 333–364.

McEwen, A.S., Eliason, E.M., Bergstrom, J.W., Bridges, N.T., Hansen, C.J., Delamere, W.A., Grant, J.A., Gulick, V.C., Herkenhoff, K.E., Keszthelyi, L., Kirk, R.L., Mellon, M.T., Squyres, S.W., Thomas, N., Weitz, C.M., 2007. Mars reconnaissance orbiter's high resolution imaging science experiment (hirise). Journal of Geophysical Research 112 (E05S02).

Mellon, M.T., Arvidson, R.E., Marlow, J.J., Phillips, R.J., Asphaug, E., 2008. Periglacial landforms at the phoenix landing site and the northern plains of mars. Journal of Geophysical Research 113 (E00A23).

Mellon, M.T., Jokosky, B.M., Postawko, S.E., 1997. The persistence of equatorial ground ice on mars. Journal of Geophysical Research 102 (E8), 19,357–19,369.

Moorman, B.J., Robinson, S.D., Burgess, M.M., 2003. Imaging periglacial conditions with ground-penetrating radar. Permafrost and Periglacial Processes 14 (4), 319–329.

Osinski, G.R., Barfoot, T.D., Ghafoor, N., Jasiobedzki, P., Tripp, J., Richards, R., Haltigin, T., Banerjee, N., Izawa, M., Auclair, S., 2008. Optimizing lunar surface activities: Lidar and msm as scientific tools? In: Proceedings of the Joint Annual Meeting of LEAG-ICEUM-SRR, pp. 4061, Cape Canaveral, Florida.

Osinski, G.R., Leveille, R., Berinstain, A., Lebeuf, M., Bamsey, M., 2007. Terrestrial analogues to mars and the moon: Canada's role. Geoscience Canada 33 (4), 175–188.

Pettinelli, E., Burghignoli, P., Pisani, A.R., Ticconi, F., Galli, A., Vannaroni, G., Bella, F., 2007. Electromagnetic propagation of gpr signals in martian subsurface scenarios including material losses and scattering. IEEE Transactions on Geoscience and Remote Sensing 45 (5), 1271–1281.

Ross, N., Harris, C., Christansen, H., Brabham, P., 2005. Ground penetrating radar investigations of open-system Pingos, Adventdalen, Svalbard. Norsk Geografisk Tidsskrift—Norwegian Journal of Geography 59, 129–138.

Seibert, N.M., Kargel, J.S., 2001. Small-scale martian polygonal terrain: Implications for liquid surface water. Geophysical Research letters 28 (5), 899–902.

Smith, D.E., Zuber, M.T., Solomon, S.C., Phillips, R.J., Head, J.W., Garvin, J.B., Banerdt, W.B., Muhleman, D.O., Pettengill, G.H., Neumann, G.A., Lemoine, F.G., Abshire, J.B., Aharonson, O., Brown, C.D., Hauck, S.A., Ivanov, A.B., McGovern, P.J., Zwally, H.J., Duxbury, T.C., 1999. The global topography of Mars and implications for surface evolution. Science 284, 1495–1503.

Smith, P.H., Tamppari, L., Arvidson, R.E., Bass, D., Blaney, D., Boynton, W., Carswell, A., Catling, D., Clark, B., Duck, T., DeJong, E., Fisher, D., Goetz, W., Gunnlaugsson, P., Hecht, M., Hipkin, V., Hoffman, J., Hviid, S., Keller, H., Kounaves, S., Lange, C.F., Lemmon, M., Madsen, M., Malin, M., Markiewicz, J., Marshall, C., McKay, C., Mellon, M., Michelangeli, D., Ming, D., Morrise, R., Renno, N., Pike, W.T., Staufer, U., Stoker, C., Taylor, P., Whiteway, J., Young, S., Zent, A., 2008. Introduction to special section on the phoenix mission: Landing site characterization experiments, mission overviews, and expected science. Journal of Geophysical Research 113 (E00A18).

Vago, J., Gardini, B., Kminek, G., Baglioni, P., Gianfiglio, G., Santovincenzo, A., Bayón, S., van Winnendael, M., 2006. ExoMars—searching for life on the Red Planet. ESA Bulletin 126, 16–23.

van Heteren, S., Fitzgerald, D.M., McKinlay, P.A., Buynevich, I.V., 1998. Radar facies of paraglacial barrier systems: Coastal new england, USA. Sedimentology 45, 181–200.

Wettergreen, D., Dias, M., Shamah, B., Teza, J., Tompkins, P., Urmson, C., Wagner, M., Whittaker, W., 2002. First experiment in sun-synchronous exploration. In: Proceedings of the IEEE International Conference on Robotics and Automation (ICRA), 3507, Washington, DC. pp. 3501.

Whiteway, J., Daly, M., Carswell, A., Duck, T., Dickinson, C., Komguem, L., Cook, C., 2008. Lidar on the phoenix mission to mars. Journal of Geophysical Research 113.

Williams, K., Grant, J., Schutz, A., 2005. Ground-penetrating radar in Mars analog terrains: Testing the strata instrument. In Workshop on Radar Investigations of Planetary and Terrestrial Environments, Houston, TX.

Zurek, R.W., Smrekar, S.E., 2007. An overview of the mars reconnaissance orbiter (mro) science mission. Journal of Geophysical Research 112 (E05S01).